IEICE TRANS. COMMUN., VOL.E106–B, NO.5 MAY 2023

PAPER

Highly Efficient Multi-Band Optical Networks with Wavelength-Selective Band Switching

Masahiro NAKAGAWA[†a)], **Hiroki KAWAHARA**[†*], **Takeshi SEKI**[†], ***Members***, ***and*** **Takashi MIYAMURA**[†], ***Senior Member***

SUMMARY Multi-band transmission technologies promise to cost-effectively expand the capacity of optical networks by exploiting low-loss spectrum windows beyond the conventional band used in already-deployed fibers. While such technologies offer a high potential for capacity upgrades, available capacity is seriously restricted not only by the wavelength-continuity constraint but also by the signal-to-noise ratio (SNR) constraint. In fact, exploiting more bands can cause higher SNR imbalance over multiple bands, which is mainly due to stimulated Raman scattering. To relax these constraints, we propose wavelength-selective band switching-enabled networks (BSNs), where each wavelength channel can be freely switched to any band and in any direction at any optical node on the route. We also present two typical optical node configurations utilizing all-optical wavelength converters, which can realize the switching proposal. Moreover, numerical analyses clarify that our BSN can reduce the fiber resource requirements by more than 20% compared to a conventional multi-band network under realistic conditions. We also discuss the impact of physical-layer performance of band switching operations on available benefits to investigate the feasibility of BSNs. In addition, we report on a proof-of-concept demonstration of a BSN with a prototype node, where C+L-band wavelength-division-multiplexed 112-Gb/s dual-polarization quadrature phase-shift keying signals are successfully transmitted while the bands of individual channels are switched node-by-node for up to 4 cascaded nodes.

key words: *multi-band optical networks, optical cross-connect, band switching, all-optical wavelength converter*

1. Introduction

High-volume and dynamic traffic is increasing year by year due to the rapid evolution of broadband access technologies and the rapid adoption of bandwidth intensive services/applications. Such traffic demand has been driving the need not only for further expansion of optical network capacity but also for more efficient use of the available spectrum resources. Recently, spectrum parallelism based on multi-band transmission has attracted much attention as a promising approach for capacity expansion; it utilizes unused wavelength bands such as O, E, S, and L bands in addition to the C band used in deployed optical fiber [1]–[4]. Since this approach enables existing fiber infrastructure to utilize expanded spectrum resources, it has the potential for cost-effective network capacity scaling.

The main goal of this work is to realize high-capacity multi-band networks that can efficiently utilize spectrum resources over multiple bands. Although such a multi-band approach offers a high potential for capacity upgrades of optical networks, the wavelength-continuity constraint and the signal-to-noise ratio (SNR) constraint must be well addressed [3]–[8]. Please note that an optical path must occupy the same wavelength (i.e., spectrum resources) on all the fiber links it traverses and the SNR performance at the receiver end must be sufficiently high for error-free operation. Moreover, if expanded spectrum resources are underutilized due to these constraints, the available network capacity cannot be expanded considerably. Therefore, we need to establish a solution that can relax both of the two constraints simultaneously.

The wavelength-continuity constraint limits the spectrum utilization because non-wavelength-continuous paths cannot be setup even if sufficient spare resources are available. This can naturally be a limiting factor for efficient spectrum utilization on multi-band networks, just as for traditional single-band ones. So far, to relax this constraint, considerable research efforts have been dedicated to leveraging all-optical wavelength converters (AO-WCs) [9], [10]. Since these studies focused only on single-band networks, it was only necessary to consider the wavelength shift of an individual channel within the same band. While such a solution can be directly applied to each band on multi-band networks, it cannot relax the SNR constraint.

The spectrum utilization on a multi-band network is seriously restricted by the SNR constraint. Specifically, on multi-band networks, SNR performance is strongly affected by inter-channel stimulated Raman scattering (ISRS). Note that ISRS is a nonlinear effect that causes a power transition from shorter to longer wavelengths during fiber propagation. Although the power tilt itself can be compensated by power equalizing techniques at the end of each span or node hop, the accumulated amount of SNR degradation can vary. Such SNR variation over multiple bands is also affected by network scale and variation in physical-layer parameters such as fiber attenuation and amplifier noise figures. Moreover, long-distance optical path setup may be blocked due to insufficient SNR on a worse-performing band. In other words, long-distance paths may not be setup even if wavelength-continuous resources are available on worse-performing bands. To respond to this multi-band-specific issue, a fiber launch power optimization method has recently been investigated for balancing SNR performance over mul-

Manuscript received April 15, 2022.
Manuscript revised August 26, 2022.
Manuscript publicized November 4, 2022.
[†]The authors are with NTT Network Service Systems Laboratories, NTT Corporation, Musashino-shi, 180-8585 Japan.
[*]Presently, with NTT Communications Corporation.
a) E-mail: masahiro.nakagawa.wh@hco.ntt.co.jp
DOI: 10.1587/transcom.2022EBP3067

tiple bands [11]. However, this method inevitably causes degradation in SNR values on better-performing bands. In fact, a remarkable degradation in SNR performance of the best-performing band can be found in [11]. This degradation can forcibly block long-distance paths on all bands. Please note that such SNR balancing cannot relax the wavelength-continuity constraint. Please also note that although optical-electrical-optical (OEO) regenerators can relax both constraints, they are costly and power hungry.

To deal with such problems, we focus on a recent advancement of AO-WC, i.e., "inter-band" AO-WC [12]. In particular, simultaneous conversion of wavelength-division-multiplexed (WDM) signals "from/to C-band to/from L-band" and "from/to C-band to/from S-band" have been successfully demonstrated. Such progressive development motivates us to consider that a wavelength shift across different bands is likely to mitigate the above-mentioned two constraints. To the best of our knowledge, this is the first work that makes use of AO-WCs for addressing both the wavelength-continuity and the ISRS-induced SNR constraints simultaneously.

Based on the above technical background, in this paper, we propose wavelength-selective band switching-enabled networks (BSNs) for efficiently utilizing spectrum resources over multiple bands. The key idea of our approach is to enable individual wavelength channels to be switched to any band and any direction at any node on the route. Adequately applying AO-WCs provides such a novel capability, which can relax the wavelength-continuity and ISRS-induced SNR constraints simultaneously. We also detail the wavelength-selective band switching functionality followed by typical node configurations. Moreover, we numerically analyze the achievable benefits of our BSN on the network resource efficiency of a multi-band network to clarify that significant fiber resource savings can be attained. Furthermore, we conduct an experimental demonstration of BSN, where 112-Gb/s/λ WDM signals over C+L-band are transmitted while switching the band for individual channels node-by-node. The main contributions of this paper are (i) presenting optical node configurations using AO-WCs for BSNs, (ii) quantitatively investigating the benefits of BSNs (i.e., the impact of relaxing both two above-mentioned constraints) through intensive numerical analysis, and (iii) experimentally demonstrating the feasibility of BSNs using the node prototype, which is extended from our previous work [13].

2. Concept

In this section, to explain the BSN concept, we give a detailed description of its novel switching functionality and its benefits to multi-band networking in terms of spectrum resource utilization.

2.1 Switching Functionality

We illustrate the switching flexibility of our BSN by contrasting it with a conventional multi-band network in Fig. 1,

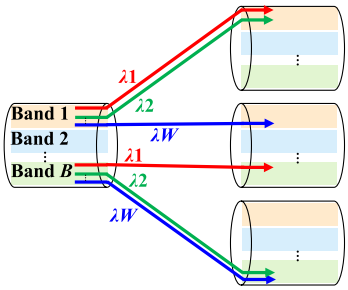

(a) Conventional multi-band networks

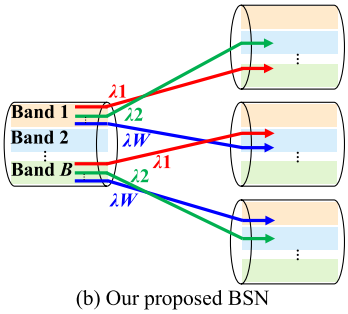

(b) Our proposed BSN

Fig. 1 Flexibility of switching of individual wavelength channels between one input and three outputs directions.

where one input and three output directions are depicted as an example. The fiber deployed for each direction is assumed to support B bands with the identical numbers of wavelength channels of W for simplicity. Note that although the available spectrum in S, E, and O bands are respectively about twice, four times, and twice as many as those in the C band, a sub-band that divides the entire band into several parts may be introduced. As shown in Fig. 1(a), on conventional multi-band networks, individual wavelength channels can be independently and freely switched to any direction but not switched across different bands. On the other hand, as shown in Fig. 1(b), individual wavelength channels can be independently switched to any band and any direction on a BSN, which enhances freedom of switching. Here, the individual wavelengths are independently converted to the wavelength with the identical wavelength index of the different band. We call such functionality "wavelength-selective band switching". In other words, we regard multiple bands on a specific fiber as multiple "spectral lanes". Thus, individual wavelength channels for each lane can be switched to different lanes by the newly defined switching functionality.

As mentioned above, wavelength-selective band switching relies on AO-WCs. For that reason, the relationship between wavelength indexes before and after conversion may change depending on the wavelength conversion scheme. For a single-stage configuration of degenerate four wave mixing (FWM) in highly nonlinear fibers (HNLFs) [12], the specific wavelength index may be converted to a different index of the different band symmetric with respect to the pump light wavelength, e.g., from index #1 to #80, from index #2 to #79, etc. On the other hand, for dual-stage configuration [14] of degenerate FWM, the specific wave-

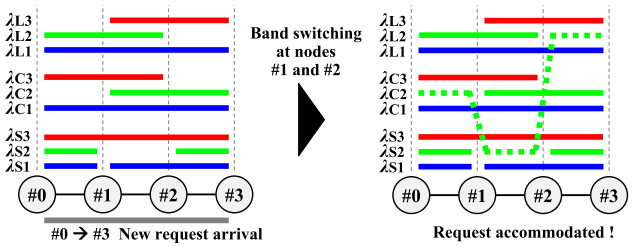

Fig. 2 Example of relaxation of the wavelength-continuity constraint.

length index may be converted directly to the identical index of the different band, e.g., from index #1 to #1, from index #2 to #2, etc. In this paper, we assume the latter case for simplicity, except for the experiment described in Sect. 5, in which AO-WC based on a single-stage configuration of degenerate FWM was utilized.

2.2 Benefits

The flexible switching capability of a BSN brings two benefits: relaxation of the wavelength-continuity constraint and relaxation of the received SNR constraint caused by ISRS. First, we describe the former as follows. An illustrative example highlighting relaxation of the wavelength-continuity constraint is shown in Fig. 2, where each link supports S, C, and L bands and each band supports three wavelength channels. Suppose that an optical path request between nodes #0 and #3 newly arrives at the initial state shown on the left in Fig. 2, but unfortunately, the 3-hop path is impossible to setup due to the wavelength-continuity constraint. However, by switching the band with the wavelength granularity at nodes #1 and #2, the new request can be accommodated utilizing residual resources, as shown on the right in Fig. 2.

Next, we describe the latter benefit, but first, we quantitatively show the impact of ISRS on transmission performance. Here, we consider a 15-THz S-, C-, and L-band 50-GHz-spaced 300-channel multi-band transmission system. Each WDM channel is Gaussian-modulated and transmitted over 10 spans of 100-km single-mode fiber (SMF) where the attenuation coefficient, dispersion, dispersion slopes, nonlinear coefficient and Raman gain slopes are 0.22 dB/km, 17 ps/nm/km, 0.067 ps/nm^2/km, 1.2 1/W/km, and 0.05 1/W/km/THz, respectively. At the end of each span, the span loss and the ISRS-induced power tilt were compensated by a thulium-doped fiber amplifier (TDFA) with a noise figure of 7 dB for the S band, and erbium-doped fiber amplifiers (EDFAs) with noise figures of 5 and 6 dB for the C and L bands, respectively. Under such system conditions, we calculated the generalized SNR (GSNR) after single span with and without ISRS using a closed form based on the ISRS GN model [6]. The GSNR after 10 spans was also calculated by adding up incoherently nonlinear interference and amplified spontaneous emission noise generated by each fiber span. The fiber launch power per channel is 0 and 2 dBm for cases with and without ISRS, respectively. Figure 3 shows the estimated GSNR as a function of the optical frequency, where the solid and dotted lines indicate the results with and without ISRS, respectively. Clearly, ISRS induces strong band-dependency on the GSNR, and S-band GSNR significantly degrades.

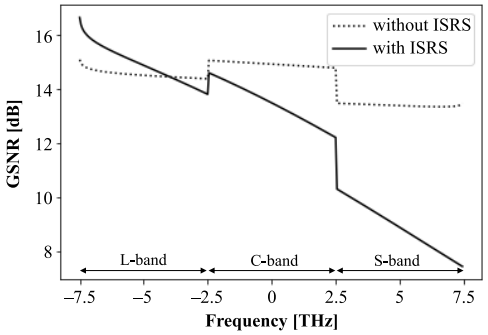

Fig. 3 GSNR after 10-span transmission with and without ISRS.

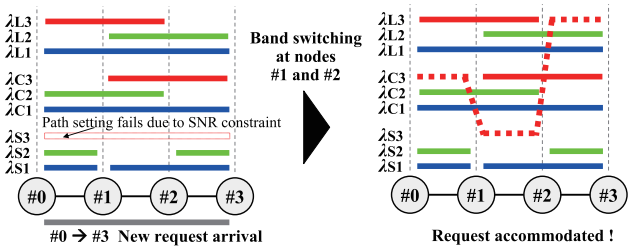

Fig. 4 Example of relaxation of the ISRS-induced SNR constraint.

This impact may block optical path provisioning as follows. Suppose that an optical path request between nodes #0 and #3 newly arrives at the initial state shown on the left in Fig. 4. Unfortunately, the 3-hop path is impossible to setup on S band if the received GSNR is insufficient due to the impact of ISRS. In this case, the new request cannot be accommodated, even if only the wavelength-continuity constraint is relaxed. However, by switching the band with the wavelength granularity at nodes #1 and #2, the new request can be accommodated utilizing residual resources of C or L band, which has a better GSNR than S band, as shown on the right in Fig. 4.

As shown in these examples, wavelength-selective band switching resolves the above-mentioned critical constraints and thus boosts multi-band network performance.

3. Optical Node Configurations

For implementing wavelength-selective band switching, optical nodes have to flexibly handle optical channels over multiple bands and enable each channel to freely select the transmission band. In this section, we present two typical node configurations which enable wavelength-selective band switching; a matrix switch-based and a wavelength-selective switch (WSS)-based configurations.

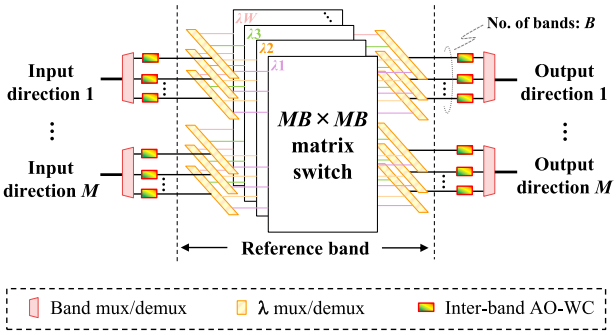

Fig. 5 Matrix switch-based configuration of OXC for a BSN.

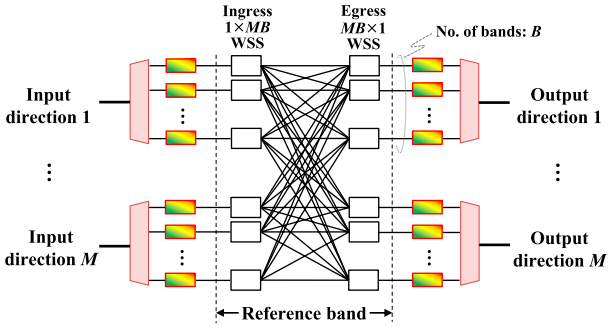

Fig. 6 WSS-based configuration of OXC for a BSN.

3.1 Matrix Switch-Based Configuration

Figure 5 shows the matrix switch-based configuration, where M is the number of directions, B is the number of bands, and W is the number of wavelengths. This optical node consists of band multiplexers and de-multiplexers (band mux/demux) for each direction, inter-band AO-WCs and wavelength multiplexers and de-multiplexers (λ mux/demux) for each band per direction, and $MB \times MB$ optical matrix switches for each wavelength. For this configuration, the optical channels across multiple bands from any input directions are band-demultiplexed, and then all channels for each band are jointly wavelength-converted to the reference band by ingress inter-band AO-WC, e.g., from O-, E-, S-, and L- to C-band. Then, multiple WDM channels with the reference band are wavelength-demultiplexed, and each wavelength channel is independently switched by the matrix switch dedicated to each wavelength, into the port connecting to the desired directions and bands. Afterwards, each wavelength channel is multiplexed in the reverse of the above process and output from the optical node. In this way, this configuration provides the new switching capability that enables individual wavelength channels to be freely switched to any band and direction. Moreover, thanks to the placement of ingress and egress inter-band AO-WC, an optical cross-connect (OXC) function (may include optical amplifiers not shown here) between the two dashed lines can be implemented only with the optical components corresponding to a reference band such as C-band.

In this configuration, the OXC function requires $2MB$ of λ mux/demux and W of $MB \times MB$ matrix switches. Here, a high-port-count optical switch can be used as multiple matrix switches. For example, a 300×300 optical switch can perform as three 100×100 switches by logical partitioning. Thus, an optical switch with a higher port count (e.g., $MBW \times MBW$) enables much simpler implementation of this configuration. Please note that such high-port-count switches and their characteristics are summarized and discussed in [15], [16]. Moreover, when we focus on fixed-grid scenarios, we can use arrayed waveguide gratings (AWGs) for λ mux/demux, which can be cost effective. However, this configuration is not suitable for the flexible-grid scenarios popular today. This is because bandwidth-variable λ mux/demux (e.g., WSSs) are required, which can result in excessive OXC loss.

3.2 Wavelength Selective Switch-Based Configuration

As a more practical approach even for flexible-grid scenarios than the previous, we describe a WSS-based configuration as shown in Fig. 6, where the λ mux/demux and matrix switch are replaced with multiple WSSs. Here, a route-and-select (R&S) type $MB \times MB$ cross-connect architecture is assumed, which is constructed by ingress $1 \times MB$ and egress $MB \times 1$ WSSs. Just as the matrix switch-based one, thanks to the placement of ingress and egress inter-band AO-WC, OXC (shown between two dashed lines) can be implemented with only the optical components corresponding to the reference band. As a result, interconnection between ingress $1 \times MB$ and egress $MB \times 1$ WSSs provides the wavelength-selective band switching without resorting to OEO conversions. The elimination of power-hungry OEO regenerators substantially improves the energy-utilization-efficiency of multi-band optical networks with conventional switching devices. Suppose that arrayed 80 OEO regenerators are installed instead of the AO-WCs in Fig. 6. With the regenerator model in [17] and assuming 100-Gb/s channel speed, the expected power consumption at the regenerators will reach 20,000 W. On the other hand, a single AO-WC, which can simultaneously handle 80 channels, will consume a few hundred W at most even when applying an optical amplifier to compensate for internal optical loss as described in [18]. Thus, the introduction of AO-WCs can suppress the power consumption for wavelength conversion by two orders of magnitude.

In addition, this configuration has a practical advantage compared to the conventional multi-band OXC node [8], in which the OXC functions for each band are deployed in parallel. Specifically, such a conventional node requires optical components other than C-band and they are generally more costly than well-established C-band ones. Our presented node does not require non-C-band components and thus prevents market fragmentation and improves market availability. In particular, the OXC shown in Fig. 6 only requires C-band WSSs, which are commonly used for commercial optical nodes. For a detailed discussion of network costs,

see the techno-economic analysis in [19].

As a further advantage, by applying multiple-arrayed WSS technology in which multiple C-band WSSs are integrated into a single optics system [20]–[22], OXC functions can be compactly implemented. Moreover, if we allow intra-node blocking, already-proposed approaches realizing cost-effective large-scale OXC (such as [23], [24]) can be applied, enabling further hardware scale reduction.

4. Numerical Analysis

In this section, to quantitatively clarify the benefits of a BSN, we numerically analyze generic BSN performance compared to a conventional multi-band network [8], where a band is assigned to each path in an end-to-end manner. On conventional multi-band networks, the same wavelength in a band must be assigned to each path on all links traversed; wavelengths in worse-performing bands cannot be assigned to long distance paths because the SNRs at multiple bands divert as the network scale increases. On the other hand, the restriction on the use of worse-performing bands can be relaxed in BSNs as paths can use wavelengths in different bands on links while impairments are caused during band-switching operations with AO-WCs. The dependency on network scale and the impairment accumulation at AO-WCs will strongly affect network performance. In order to evaluate the trade-offs between these factors, the total transmission penalties are estimated for both networks and the performance is evaluated subject to these penalties. Following, we first describe the assumed model and metric for analysis. Second, our analysis procedure is provided. Then, we explore the maximum potential benefits of a BSN enabled by wavelength-selective band switching. The impact of physical-layer performance of band switching operations on the attainable benefits is also discussed to investigate the feasibility of BSNs.

4.1 Assumptions

We assume a 3×3 poly-grid network (see Fig. 7) as the topology tested. Moreover, S+C+L bands can be operated on each link, where each link length is equal to D and a span length of 100 km is assumed. Since it has been reported that the average link length of 40 real optical transport networks is about 400 km [25], D is set to be around 400 km, i.e., 300, 400, or 500 km. In addition, we use physical parameters of each link summarized in Sect. 2.2 for realistic evaluations. On each link, the same amount of spectrum resources (e.g., 4.5 THz) are available in each band for simplicity.

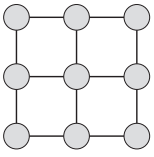

Fig. 7 3 × 3 poly-grid network topology.

In this work, comparisons of network performance are provided using the metric of the amount of required fiber resources for accommodating a particular traffic demand. Note that such a metric is often used to discuss spectrum utilization efficiency. To keep discussions as simple as possible while evaluating BSN benefits from a broad perspective, we estimate a lower bound of required fiber resources. For each path setup demand, we find a set of valid band-assignment candidates, which are vectors of link numbers on which the path occupies corresponding bands; for example, a candidate (i, j, k) stands for the transmission over i, j, k links respectively on S, C, L bands. We first select the one candidate minimizing the transmission margin for each demand. Note that this selection strategy is a reasonable for efficient spectrum utilization as discussed in [26]. Then, according to selected candidates, we calculate the total spectrum usage of each band by summing up individual demands' spectrum usage. The spectrum usage of an individual demand on S, C, L bands are represented by the product of the required spectrum and selected values of i, j, k, respectively. Afterwards, we try to minimize the required fiber resources to accommodate all the demands through an iterative optimization approach, where the band-assignment candidates are changed to reduce the fiber amount considering the spectrum usage of each band. Here we omit the routing and wavelength/spectrum assignment (RWA/RSA), the solution given by this procedure gives a lower bound of the required fiber resources, F_{bound}, from the spectrum usage and available spectrum per fiber, expressed as

$$F_{bound} = \max\left(\frac{U_S}{A_S}, \frac{U_C}{A_C}, \frac{U_L}{A_L}\right),$$

where U_S, U_C, and U_L denote the total spectrum usage of S-, C-, and L-bands, respectively, while A_S, A_C, and A_L denote available spectrum per fiber of S-, C-, and L-bands, respectively. Please note that imbalance in spectrum usage over multiple bands can increase the lower bound. In other words, valuable fiber resources can be saved if well-balanced spectrum usage is achieved even when considering band-dependent transmission performance. Also note that each demand requires 100-Gb/s capacity and the modulation format used is 32 Gbaud dual-polarization quadrature phase-shift keying (DP-QPSK) with 50-GHz spacing in this analysis.

4.2 Procedure

In our analysis, for a given traffic demands, the minimum value of F_{bound} is derived based on the simplex method, which is a well-known method for solving linear programming problems. In particular, we first select a band-assignment candidate for each demand to obtain an initial feasible solution, and then we iteratively improve the solution using an exhaustive search until convergence. In more detail, our analysis consists of the following steps.

Step 1. A sufficient number of demands are generated according to the distribution and intensity of demands

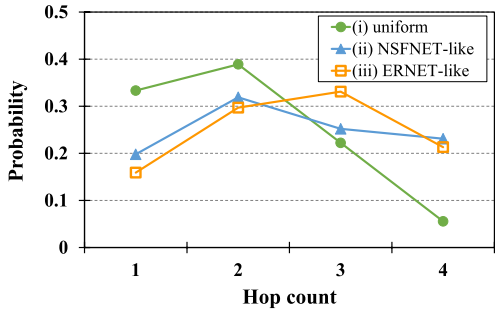

Fig. 8 Assumed hop count distribution.

given in advance.

Step 2. For each demand, a band-assignment candidate that minimizes the transmission margin is selected. Please note that this step enables acquisition of the initial solution (i.e., band usage for each demand).

Step 3. U_S, U_C, and U_L are calculated with the procedure in Sect. 4.1. Moreover, F_{bound} at the time is also calculated, according to the formula in Sect. 4.1.

Step 4. All possible adjacent solutions in which the band assignment for only one demand is changed are searched. In addition, the improvement amount (i.e., a decrease in the F_{bound} value) attained by replacing the current solution with each adjacent solution is calculated.

Step 5. If no adjacent solution can improve the current solution, then the process is terminated. Otherwise, go to step 6.

Step 6. The current solution is replaced by the best adjacent solution that offers the largest improvement.

Step 7. Values of U_S, U_C, U_L, and F_{bound} are updated, just as step 3. Then, go to step 4.

Finally, we compare the derived values of F_{bound} between our BSN and a conventional one.

Please note that the hop count, i.e., path length of each demand, is determined in step 1, according to the following three probability distributions; (i) *uniform*, (ii) *NSFNET-like*, and (iii) *ERNET-like*, as illustrated in Fig. 8. Since we ignore the RWA/RSA in this analysis as previously mentioned, hop count distribution is a crucial parameter for describing the traffic characteristics. Please note that *uniform* assumes the case when source/destination pair of each demand follows a uniform distribution, and its average hop count is 2. The other two represent actual path length distributions in real network topologies of NSFNET and ERNET [27]. In particular, it has been reported that the shortest path length distribution of real optical networks can be accurately modeled by using Johnson S_B distribution [27], which enables recreation of realistic distributions with parameter values reported in [27]. Moreover, we discretize them to derive the distributions in Fig. 8. The average hop count of *NSFNET-like* and *ERNET-like* are 2.5 and 2.6, respectively.

Please also note that, in steps 2 and 4, transmission performance and its margin are expressed by the GSNR as described in Sect. 2.2. Specifically, according to [6], the attainable GSNR can be calculated by using the per-span GSNR information for each band. Just as in Sect. 2.2, the fiber launch power per channel is set to 0 dBm, and the calculated worst-case GSNR values after a 100-km single span transmission are summarized in Table 1. Note that this launch power setting aims to suppress GSNR degradation in better-performing bands, which allows long-distance paths to be setup with sufficient quality. Moreover, a GSNR margin is defined as the difference between the attainable GSNR and minimum GSNR required for error-free transmission. According to [4], assuming the pre-forward error correction (FEC) bit error rate (BER) limit of 4×10^{-3}, the minimum required GSNR for DP-QPSK is set to be 8.5 dB.

Table 1 Worst-case GSNR after 100-km single span transmission.

Scenario	S-band	C-band	L-band
C-band only	–	24.38 dB	–
S+C+L-band	17.45 dB	22.26 dB	23.9 dB

4.3 Results and Discussion

The calculated minimum F_{bound} values for 10,000 demands are shown in Fig. 9, where each of A_S, A_C, and A_L is assumed to be 4.5 THz. Although these results may be extreme examples, they can make it easy understand the behavior of F_{bound} when link length and/or traffic pattern is varied. The results reveal that the link length strongly affects the required fiber resources in a conventional multi-band network. In particular, when the link length becomes longer (i.e., when changed from 300 km to 400 km), F_{bound} values increase in a conventional network for all the traffic patterns. This is because the worst-performing S band cannot be used for long-distance path setup, which causes imbalance in spectrum usage over multiple bands. On the other hand, in a BSN, remarkable increase in F_{bound} is not observed when the link length increases. These results suggest that except for small-scale networks, our BSN is necessary for efficient multi-band spectrum utilization.

Moreover, the ratio of the minimum F_{bound} achieved by a BSN to that attained by a conventional network is calculated for each network scale and traffic pattern, as shown in Fig. 10. Please note that the transmission penalty induced by band switching is not considered in Figs. 9 and 10 for exploring the maximum potential benefits of a BSN. The results verify that our BSN can significantly save fiber resources especially when D is 400 km (average scale) or 500 km (larger scale). In such cases, BSN can reduce fiber resources by more than 20% compared to a conventional one in any traffic patterns tested. This is mainly because a BSN can flexibly utilize spectrum over multiple bands, which enables spectrum usage equalization among S-, C-, and L-bands, even on large-scale networks.

When focusing on the impact of traffic patterns, it is found that the improvement amount achieved by a BSN tends to increase with the average hop count (i.e., the average path length). This is because the increase in the average path length causes more imbalanced band usage on conven-

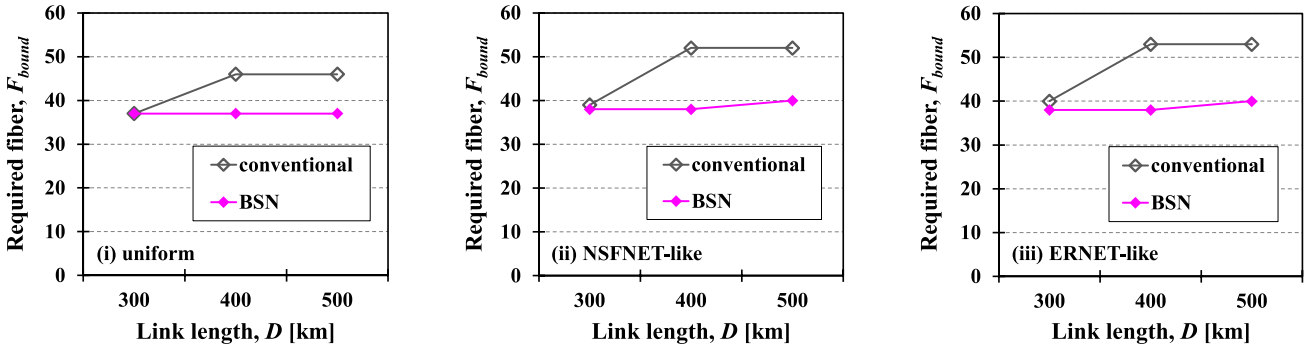

Fig. 9 Calculated number of required fibers.

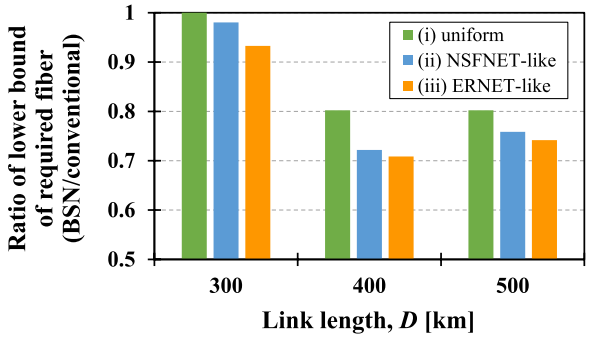

Fig. 10 Ratio of required fiber resources.

tional multi-band networks, where the worst-performing S band is used less while the best-performing L band is used more. Moreover, if we focus on *NSFNET-like* and *ERNET-like* patterns, we observe that the calculated ratio in the larger-scale scenario (D = 500 km) is slightly larger than that in the average-scale scenario (D = 400 km). This can be explained by the fact that better-performing C and L bands usage on a BSN also gradually increase when the average path length rises above a certain level. Such results imply that our analysis is fair and reasonable.

Remark: When applying a power optimization method for balancing GSNR performance over all the bands (e.g., presented in [11], which forces the worst-case GSNR values per span for all bands to be more than 3.6 dB lower than that in a C-band-only case under the assumed condition) in this analysis, the longest path cannot be setup due to margin shortage in the average-scale and larger-scale scenarios. Therefore, such an approach is not suitable on large core networks although it can simplify multi-band RWA/RSA problems on smaller-scale networks.

Furthermore, to clarify the viability of a BSN, we evaluate network performance in consideration of the GSNR penalty induced by the wavelength-selective band switching. Actually, the AO-WC induced transmission penalty and its impact on network performance are of concern for practical use. In general, physical layer performance of AO-WCs depends on various factors such as mechanisms for wavelength conversion and implementation. In our analysis, the GSNR penalty per band switching operation is introduced

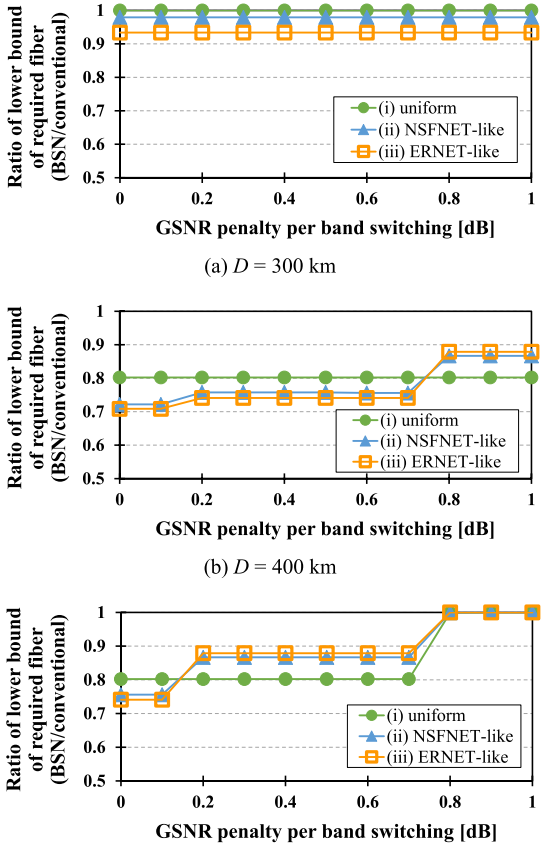

(a) D = 300 km

(b) D = 400 km

(c) D = 500 km

Fig. 11 Impact of GSNR penalty induced by band switching operations.

as a parameter in estimating the attainable GSNR. In particular, the product of the GSNR penalty per band switching and the number of band-switching operations is simply subtracted from the original attainable GSNR value. In this way, the ratios of the fiber-resource lower bounds as a function of GSNR penalty per band switching are shown in Fig. 11. The results indicate that a large improvement can be obtained even considering the band switching induced penalty. For instance, when the GSNR penalty per band switching is lower than 0.7 dB, a BSN can save fiber resources by more than 20% and 12% in the average-scale and larger-scale scenarios, respectively. Please note that a

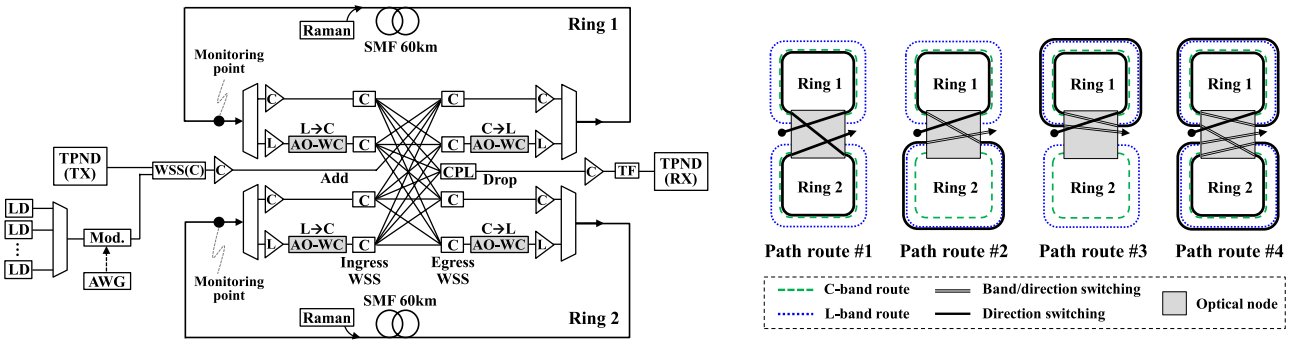

(a) (b)

Fig. 12 (a) Experimental setup. (b) Path setting patterns to emulate band switching with wavelength granularity node-by-node.

GSNR penalty of less than 0.7 dB may be a possible value, which is experimentally verified in Sect. 5. These analysis results successfully verify that our BSN is beneficial under a wide range of conditions in terms of network scale and traffic patterns.

5. Experimental Demonstration

This section presents a proof-of-concept experiment showing the feasibility of a BSN by emulating a multi-band network with our presented WSS-based optical node configuration. Moreover, we demonstrate multiple node-traversing transmission with node-by-node wavelength-selective band switching.

5.1 Setup

Figure 12(a) shows the experimental setup, where a 2-degree optical node supporting C+L bands is configured. We assume that two unidirectional rings are connected by this optical node. Moreover, multiple transmitters and a single receiver are used for the transmission experiment. In the node configuration, C- and L-band EDFAs were deployed at input and output ports as pre- and post-amplifiers, respectively. We prototyped an inter-band AO-WC based on degenerate FWM in a HNLF and implemented it in a similar manner to that in [12]. At this moment, each AO-WC actually has the insertion loss (also called conversion loss) of about 20 dB, and thus a C- or L-band EDFA is deployed within each AO-WC to compensate for the loss, just as in [18]. Egress WSSs equalized the wavelength-dependent gain of the inter-band AO-WC and EDFA. Each ring consisted of a 60-km SMF and a C-band backward distributed Raman amplifier to compensate for the power tilt arising from ISRS. Note that this link length is shorter than that assumed in Sect. 4, where the impact of long distance transmission on multi-band network performance was highlighted. Alternatively, in this experiment, we focus on physical-layer feasibility of our node configuration and band switching operation considering actual AO-WC performance.

At the transmitter side, 50-GHz-spaced 72-channel 112-Gbit/s DP-QPSK signals ranging from 1529.55 to 1556.96 nm were generated, and one channel of them was replaced with the signal output from a real-time transponder (TPND). The C-band WDM signal was added to the node and launched into the ring 1 route. After the first span transmission, the optical node delivered individual wavelength channels to ring 1 or 2 by directional switching and to C- or L-band routes by band switching. The channel launch power was 3 dBm/ch at rings 1 and 2.

Figure 12(b) shows the path setting patterns in consideration of band switching with wavelength granularity node-by-node. Please note that the green dashed and blue dotted lines denote the C- and L-band routes, and the black solid line shows the path routes corresponding to patterns #1–#4 that are assigned to every 4 channels of the 72-channel WDM signal. The C- and L-band WDM signal spectra were observed at the end of rings. Through an optical coupler for the drop, EDFA, and tunable filter (TF), individual channels within the C-band WDM signal were incident into the receiver, and the Q-factor was measured in real-time.

5.2 Results

Figure 13 shows overall and expanded spectra monitored at the ends of ring 1 and 2, which represent the basic characteristics of wavelength-selective band switching at the optical node configured. For instance, the wavelength channel assigned for path setting #4 was transmitted in C-band ring 1 route for the first span, L-band ring 1 route for second span, C-band ring 2 route for third span, and L-band ring 2 route for fourth span.

Moreover, Q factors and penalties as a function of channel wavelength are shown in Fig. 14. The Q penalties were calculated by subtracting the measured Q factors from the pre-measured back-to-back Q factors at the same OSNR. The Q factors of all 72 channels greatly exceed the Q limit of 5.2 dB. However, there were moderate penalties of < 0.5 dB, < 1.4 dB, < 1.4 dB, and < 2.4 dB for path settings #1–#4, respectively. Please note that the numbers of AO-WC traversed by such settings #1–#4 are 0, 2, 2, and 4, respectively.

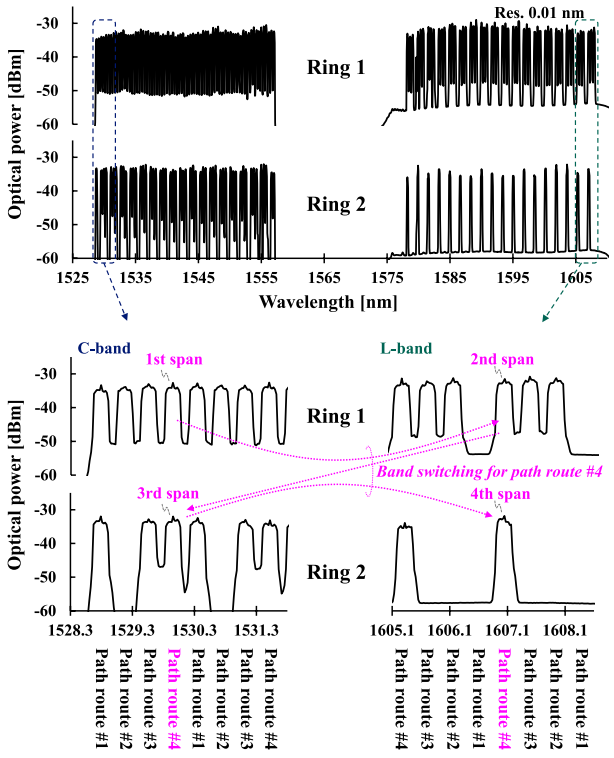

Fig. 13 Overall (top) and expanded (bottom) optical signal spectra monitored at the ends of rings 1 and 2.

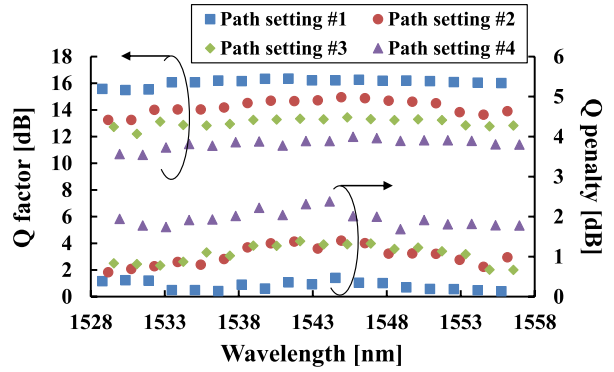

Fig. 14 Measured Q factor and Q penalty.

These imply that the predominant factor for measured penalties was the nonlinearity inside the AO-WC operating in the multiple wavelength condition. However, the obtained results indicate that the penalty per band switching of less than 0.7 dB can be a possible value. This provides good evidence for the actual effectiveness of our BSN. Specifically, in the previous section, it was illustrated that our BSN can significantly improve network performance if the penalty per band switching is suppressed less than 0.7 dB (see Fig. 11). Furthermore, we believe that such AO-WC-induced penalties can be suppressed by finely tuning the FWM generation condition.

As a consequence, we confirmed that sufficiently high-quality signal transmission while switching the bands of individual channels node-by-node can be achieved for up to 4 cascaded nodes. This successfully demonstrated the feasibility of a BSN for a C+L-band scenario, which is an important step for efficient multi-band networking. Moreover, thanks to progressive development of AO-WC [18], [28], [29], it is expected that the feasibility of band switching operation will be improved in terms of operation band and amount of penalty. For instance, in [18], C-to-L, L-to-C, C-to-S, and S-to-C AO-WCs have been demonstrated, in which each AO-WC has almost the same conversion loss. In [28], [29], the improved conversion-loss performance has been demonstrated. Such efforts will increase viability and practicality of our BSN.

6. Conclusions

This paper proposed wavelength-selective band switching-enabled networks (BSNs) for viable network capacity scaling. In BSNs, we can efficiently utilize expanded network resources through multi-band transmission technology since both the wavelength-continuity and ISRS-induced SNR constraints can be relaxed. To the best of our knowledge, this is the first solution that can simultaneously relax the above two constraints in multi-band scenarios without the need for OEO regenerators. We also presented two typical optical node configurations that provide the new functionality of wavelength-selective band switching. In these configurations, the WDM signals for each band are jointly converted to and from a reference band such as C-band by ingress and egress inter-band AO-WCs. This configuration concept enables OXC functionality to be implemented with only commonly available C-band components. As a result, OXC for each band signal can be fully interconnected, which realizes switching functionality. Numerical analysis revealed that a BSN can potentially save valuable fiber resources by more than 20% compared to a conventional multi-band network. This is mainly because the worst-performing band resources can be efficiently utilized by relaxing the ISRS-induced SNR constraint. Moreover, we conducted a proof-of-concept experiment of a BSN by emulating the proposed network with our node prototype. The experimental results showed that high-quality transmission of C+L-band WDM DP-QPSK signals can be achieved while switching bands of individual channels node-by-node for up to 4 cascaded nodes. These results confirm the feasibility of our BSN.

Acknowledgments

The authors would like to thank Prof. Hasegawa from Nagoya University for fruitful discussion.

References

[1] J. Renaudier, A.C. Meseguer, A. Ghazisaeidi, P. Tran, R.R. Muller, R. Brenot, A. Verdier, F. Blache, K. Mekhazni, B. Duval, H. Debregeas, M. Achouche, A. Boutin, F. Morin, L. Letteron, N. Fontaine, Y. Frignac, and G. Charlet, "First 100-nm continuous-band

WDM transmission system with 115 Tb/s transport over 100 km using novel ultra-wideband semiconductor optical amplifiers," Proc. ECOC, paper Th.PDP.A.3, Sept. 2017.
[2] A. Napoli, N. Calabretta, J.K. Fischer, N. Costa, S. Abrate, J. Pedro, V. Lopez, V. Curri, D. Zibar, E. Pincemin, S. Grot, G. Roelkens, C. Matrakidis, and W. Forysiak, "Perspectives of multi-band optical communication systems," Proc. OECC, paper 5B3-1, July 2018.
[3] F. Hamaoka, M. Nakamura, S. Okamoto, K. Minoguchi, T. Sasai, A. Matsushita, E. Yamazaki, and Y. Kisaka, "Ultra-wideband WDM transmission in S-, C-, and L-bands using signal power optimization scheme," J. Lightw. Technol., vol.37, no.8, pp.1764–1771, April 2019.
[4] N. Sambo, A. Ferrari, A. Napoli, N. Costa, J. Pedro, B. Sommerkorn-Krombholz, P. Castoldi, and V. Curri, "Provisioning in multi-band optical networks," J. Lightw. Technol., vol.38, no.9, pp.2598–2605, May 2020.
[5] S. Okamoto, K. Minoguchi, F. Hamaoka, K. Horikoshi, A. Matsushita, M. Nakamura, E. Yamazaki, and Y. Kisaka, "A study on the effect of ultra-wide band WDM on optical transmission systems," J. Lightw. Technol., vol.38, no.5, pp.1061–1070, March 2020.
[6] D. Semaru, R.I. Killey, and P. Bayvel, "A closed-form approximation of the Gaussian noise model in the presence of inter-channel stimulated Raman scattering," J. Lightw. Technol., vol.37, no.9, pp.1924–1936, May 2019.
[7] A. Ferarri, E. Virgillito, and V. Curri, "Band-divison vs. space-division multiplexing: A network performance statistical assessment," J. Lightw. Technol., vol.38, no.5, pp.1041–1049, March 2020.
[8] A. Ferrari, A. Napoli, J.K. Fischer, N. Costa, A. D'Amico, J. Pedro, W. Forysiak, E. Pincemin, A. Lord, A. Stavdas, J.P.F.-P. Gimenez, G. Roelkens, N. Calabretta, S. Abrate, B. Sommerkorn-Krombholz, and V. Curri, "Assessment on the achievable throughput of multi-band ITU-T G.652.D fiber transmission systems," J. Lightw. Technol., vol.38, no.16, pp.4279–4291, Aug. 2020.
[9] J.M. Yates and M.P. Rumsewicz, "Wavelength converters in dynamically-reconfigurable WDM networks," IEEE Commun. Surveys Tuts., vol.2, no.2, pp.2–15, Second Quarter 1999.
[10] K. Ishii, T. Inoue, I. Kim, X. Wang, H.N. Tan, Q. Zhang, T. Ikeuchi, and S. Namiki, "Analysis and demonstration of network utilization improvement through format-agnostic multi-channel wavelength converters," J. Opt. Commun. Netw., vol.10, no.2, pp.A165–A174, Feb. 2018.
[11] D. Uzunidis, C. Matrakidis, A. Stavdas, and A. Lord, "Power optimization strategy for multi-band optical systems," Proc. ECOC, paper Tu1H-4, Dec. 2020.
[12] T. Kato, S. Watanabe, T. Yamauchi, G. Nakagawa, H. Muranaka, Y. Tanaka, Y. Akiyama, and T. Hoshida, "Real-time transmission of 240 × 200-Gb/s signal in S+C+L triple-band WDM without S- or L-band transceivers," Proc. ECOC, paper PD.1.7, Sept. 2019.
[13] H. Kawahara, M. Nakagawa, T. Seki, and T. Miyamura, "Experimental demonstration of wavelength-selective band/direction-switchable multi-band OXC using an inter-band all-optical wavelength converter," Proc. ECOC, paper Tu1H.3, Dec. 2020.
[14] H.N. Tan, T. Inoue, K. Solis-Trapala, S. Petit, Y. Oikawa, K. Ota, S. Takasaka, T. Yagi, M. Pelusi, and S. Namiki, "On the cascadability of alloptical wavelength converter for high-order QAM formats," J. Lightw. Technol., vol.34, no.13, pp.3194–3205, July 2016.
[15] M. Stepanovsky, "A comparative review of MEMS-based optical cross-connects for all-optical networks from the past to the present day," IEEE Commun. Surveys Tuts., vol.21, no.3, pp.2928–2946, Third Quarter 2019.
[16] Y. Mori and K. Sato, "High-port-count optical circuit switches for intra-datacenter networks," J. Opt. Commun. Netw., vol.13, no.8, pp.D43–D52, Aug. 2021.
[17] J. Zhang, Y. Zhao, X. Yu, J. Zhang, M. Song, Y. Ji, and B. Mukherjee, "Energy-efficient traffic grooming in sliceable-transponder-equipped IP-over-elastic optical networks," J. Opt. Commun. Netw., vol.7, no.1, pp.A142–A152, Jan. 2015.
[18] T. Kato, S. Watanabe, T. Yamauchi, G. Nakagawa, H. Muranaka, Y. Tanaka, Y. Akiyama, and T. Hoshida, "Multi-band WDM transmission technology exceeding transceiver wavelength band," Proc. OECC, paper T1-4.1, Dec. 2020.
[19] M. Nakagawa, T. Seki, and T. Miyamura, "Techno-economic potential of wavelength-selective band-switchable OXC in S+C+L band optical networks," Proc. OFC, paper W2A.24, March 2022.
[20] K. Suzuki, K. Seno, and Y. Ikuma, "Application of waveguide/free-space optics hybrid to ROADM device," J. Lightw. Technol., vol.35, no.4, pp.596–606, Feb. 2017.
[21] H. Kawahara, A. Sahara, Y. Sone, S. Kawai, M. Fukutoku, and Y. Miyamoto, "First investigation and reduction of inter-WSS crosstalk in multiple-arrayed WSSs for large-scale optical node," Proc. CLEO-PR/OECC/PGC, paper 3-2K-2, July/Aug. 2017.
[22] H. Yang, P. Wilkinson, B. Robertson, S. Giltrap, O. Snowdon, H. Prudden, and D. Chu, "24 [1 × 12] wavelength selective switches integrated on a single 4k LCoS device," J. Lightw. Technol., vol.39, no.4, pp.1033–1039, Feb. 2021.
[23] A. Sahara, H. Kawahara, S. Yamamoto, S. Kawai, M. Fukutoku, T. Mizuno, Y. Miyamoto, K. Suzuki, and K. Yamaguchi, "Proposal and experimental demonstration of SDM node enabling path assignment to arbitrary wavelengths, cores, and directions," Opt. Express, vol.25, no.4, pp.4061–4075, Feb. 2017.
[24] Y. Iwai, H. Hasegawa, and K. Sato, "A large-scale photonic node architecture that utilizes interconnected OXC subsystems," Opt. Express, vol.21, no.1, pp.478–487, Jan. 2013.
[25] S.K. Routray, R. Morais, J.R.F. da Rocha, and A.N. Pinto, "Statistical model for link lengths in optical transport networks," J. Opt. Commun. Netw., vol.5, no.7, pp.762–773, July 2013.
[26] M. Jinno, "Elastic optical networking: Roles and benefits in beyond 100-Gb/s era," J. Lightw. Technol., vol.35, no.5, pp.1116–1124, March 2017.
[27] S.K. Routray, G. Sahin, J.R.F. da Rocha, and A.N. Pinto, "Statistical analysis and modeling of shortest path lengths in optical transport networks," J. Lightw. Technol., vol.33, no.13, pp.2791–2801, July 2015.
[28] T. Umeki, O. Tadanaga, and M. Asobe, "Highly efficient wavelength converter using direct-bonded PPZnLN ridge waveguide," IEEE J. Quantum Electron., vol.46, no.8, pp.1206–1213, Aug. 2010.
[29] C. Wang, C. Langrock, A. Marandi, M. Jankowski, M. Zhang, B. Desiatov, M.M. Fejer, and M. Lončar, "Ultrahigh-efficiency wavelength conversion in nanophotonic periodically poled lithium niobate waveguides," OSA Optica, vol.5, no.11, pp.1438–1441, Nov. 2018.

Masahiro Nakagawa received the B.E. and M.E. degrees in Electrical Engineering and Computer Science from Nagoya University, Aichi, Japan, in 2008 and 2010, respectively. In 2010, he joined NTT Corporation, Tokyo, Japan. Currently, he is with NTT Network Service Systems Laboratories, where he is engaged in research and development on transport network systems. His research interests include photonic network systems. He is a Member of the Institute of Electronics, Information and Communication Engineers of Japan.

Hiroki Kawahara received the B.E. and M.E. degrees in electrical, electronics, and information engineering from Osaka University, Osaka, Japan, in 2009 and 2011, respectively. He is currently with Nippon Telegraph and Telephone Corporation, where his work involves optical cross-connect and optical transmission systems. He is a Member of the Institute of Electronics, Information and Communication Engineers of Japan.

Takeshi Seki received the B.S. and M.S. degrees in electronics and applied physics from Tokyo Institute of Technology, Tokyo, Japan, in 2002 and 2004, respectively. In 2004, he joined the Nippon Telegraph and Telephone (NTT) Network Service Systems Laboratories, where he got engaged in research on optical cross-connect systems. He is currently developing WDM transmission systems in NTT Network Service Systems Laboratories. He is a Member of the Institute of Electronics, Information and Communication Engineers of Japan.

Takashi Miyamura is a Senior Researcher, Supervisor and Research Group Leader at NTT Network Service Systems Laboratories, Tokyo Japan. He received the B.S. and M.S. degrees from Osaka University, Osaka, Japan in 1997 and 1999, respectively, and Ph.D. degree from Hokkaido University in 2018. In 1999, he joined NTT Network Service Systems Laboratories, where he engaged in research and development of a high-speed IP switching router. He is now researching future optical transport network architectures and an optical switching system. He received paper awards from the 7th Asia-Pacific Conference on Communications (APCC 2001), and best paper award from the 19th Asia-Pacific Network Operations and Management Symposium (APNOMS 2017). He is a senior member of IEICE, and a member of IEEE.